Supporting Information for:

Synthesis of Promising Metal Oxide Light Absorber $CuBiW_2O_8$ (CBTO) by Cu-Rich Solid State Method and Measurement of Optoelectronic Properties

Lite Zhou[†,1,2], Edan Bainglass[†,3], Maryam Masroor[1,2], Binod Giri[1,2], Guangjiang Li[4], Alexander Carl[5], Ronald L. Grimm[5], Muhammad N. Huda[3], Lyubov V Titova[4], and Pratap M. Rao[1,2]*

[†]Equal contributions

[1]Department of Mechanical Engineering, Worcester Polytechnic Institute, Worcester, Massachusetts, 01609, United States

[2]Materials Science and Engineering Graduate Program, Worcester Polytechnic Institute, Worcester, Massachusetts, 01609, United States

[3]Department of Physics, University of Texas at Arlington, Arlington Texas, 76019, United States

[4]Department of Physics, Worcester Polytechnic Institute, Worcester, Massachusetts, 01609, United States

[5]Department of Chemistry and Biochemistry, Worcester Polytechnic Institute, Worcester, Massachusetts, 01609, United States

Methods of Theoretical Calculations

Ground state energy calculations were carried out in the Vienna *ab initio* Simulation package (VASP 5.4.4)[1, 2] using the generalized gradient approximation as parameterized by Perdew-Burke-Ernzerhof (GGA-PBE)[3, 4] to handle the exchange and correlation potential of the Kohn-Sham equations of DFT[5]. Core electrons were treated within the frozen-core projector augmented-wave (PAW) framework[6, 7], while valence electrons were expanded in a plane wave basis set with a kinetic energy cutoff of 600 eV. Integrations in the Brillouin zone (BZ) were performed without symmetry considerations using the 2nd order Methfessel-Paxton method[8] on Monkhorst-Pack[9] k-point meshes derived from lattice shapes and sizes. Energy cutoff and k-point mesh values were converged within a total energy of 1 meV for all compound. As was done in the original theoretical work on CBTO[10], a Hubbard-U[11-13] on-site Coulomb potential of U_{eff} = 6 eV was applied to Cu 3d to correct the underestimation of d-electron localization by DFT[11, 14, 15]. The same was applied to all Cu-containing fragments.

The single-phase region of a chemical potential landscape is obtained by solving a system of inequalities reflecting enthalpic conditions for the primary compound and any of its possible secondary phases,

$$\sum_{\alpha} n_{\alpha}\Delta\mu_{\alpha} = \Delta H_{f,p} \qquad (S1a)$$

$$\sum_{\beta} n_{\beta}\Delta\mu_{\beta} < \Delta H_{f,s} \qquad (S1b)$$

as functions of chemical potentials of species constituting the primary phase[16]. In the above equations, $n_{\alpha,\beta}$ and $\Delta\mu_{\alpha,\beta}$ respectively represent the fractions of each species in the formula unit and its chemical potential bounded by

$$\Delta H_f \leq n_{\alpha,\beta}\Delta\mu_{\alpha,\beta} \leq 0 \qquad (S2)$$

ΔH_f is the calculated formation enthalpy of the primary/secondary phase derived from E_{solid}, the total ground state energy of the compound,

$$\Delta H_f = E_{solid} - \sum_{\alpha} n_{\alpha} E_{\alpha}^{bulk} \qquad (S3)$$

where E_{α}^{bulk} is the ground state energy of α in its standard elemental phase. For CBTO, the process involves the following system of inequalities:

$$\mu_{Cu} + \mu_{Bi} + 2\mu_W + 4\mu_{O_2} = \Delta H_{f,CBTO} = -21.386\ eV \quad (S4a)$$

$$\mu_{Cu} + \mu_{O_2} < \Delta_{f,CuO} = -1.590\ eV \quad (S4b)$$

$$2\mu_{Cu} + \frac{1}{2}\mu_{O_2} < \Delta_{f,Cu_2O} = -1.602\ eV \quad (S4c)$$

$$2\mu_{Bi} + \frac{3}{2}\mu_{O_2} < \Delta_{f,Bi_2O_3} = -6.242\ eV \quad (S4d)$$

$$\mu_W + \frac{3}{2}\mu_{O_2} < \Delta_{f,WO_3} = -8.588\ eV \quad (S4e)$$

$$\mu_{Cu} + \mu_W + 2\mu_{O_2} < \Delta_{f,CuWO_4} = -10.253\ eV \quad (S4f)$$

$$2\mu_{Cu} + \mu_W + 2\mu_{O_2} < \Delta_{f,Cu_2WO_4} = -10.013\ eV \quad (S4g)$$

$$2\mu_{Bi} + \mu_W + 3\mu_{O_2} < \Delta_{f,Bi_2WO_6} = -15.547\ eV \quad (S4h)$$

Solutions to the above equations with Cu taken as a free variable are shown in Figure 2 of the main text. Similar analyses for Bi and W are shown here in Figure S1a and S1b, respectively. Defect formation enthalpies are given by

$$\Delta H_\delta = E_\delta - E_p + \sum\nolimits_\alpha m_\alpha \mu_\alpha \quad (S6a)$$

$$\mu_\alpha = \mu_\alpha^0 + \Delta\mu_\alpha \quad (S6b)$$

where E_δ and E_p are the total ground state energies of the primary compound with and without the defect, respectively. By convention, $m_\alpha = -1$ corresponds to the addition of one α atom to the system. μ_α^0 is a reference chemical potential from the standard elemental phase of α. $\Delta\mu_\alpha$ determines the chemical environment by representing the additional energy required to get α from a source during synthesis, with $\Delta\mu_\alpha = 0$ reflecting α-rich conditions. $\Delta\mu_\alpha$ is bounded according to eq. S2.

The frequency dependent absorption coefficient $\alpha(\omega)$ is derived from the extinction coefficient $k(\omega)$ as follows[17]:

$$\alpha_{ii}(\omega) = \frac{2\omega}{c} k_{ii}(\omega) \quad (S7a)$$

$$k_{ii}(\omega) = \left\{\frac{1}{2}\left[\left[\left(\mathrm{Re}\ \varepsilon_{ii}(\omega)\right)^2 + \left(\mathrm{Im}\ \varepsilon_{ii}(\omega)\right)^2\right]^{1/2} - \mathrm{Re}\ \varepsilon_{ii}(\omega)\right]\right\}^{1/2} \quad (S7b)$$

where c is the speed of light, and the real and imaginary parts of $\varepsilon(\omega)$, the dielectric tensor, are calculated from the following[18]:

$$\mathrm{Im}\ \varepsilon_{ij}(\omega) = \frac{4\pi^2 e^2}{\Omega} \lim_{q\to 0} \frac{1}{q^2} \sum\nolimits_{c,v,\boldsymbol{k}} 2w_{\boldsymbol{k}} \delta(\varepsilon_{c\boldsymbol{k}} - \varepsilon_{v\boldsymbol{k}} - \omega) \times \langle u_{c\boldsymbol{k}+\boldsymbol{e}_i q} | u_{c\boldsymbol{k}} \rangle \langle u_{c\boldsymbol{k}+\boldsymbol{e}_j q} | u_{c\boldsymbol{k}} \rangle \quad (S8a)$$

$$\text{Re}\ \varepsilon_{ij}(\omega) = 1 + \frac{2}{\pi} P \int_0^{\infty} \frac{\text{Im}\ \varepsilon_{ij}(\omega')\omega'}{\omega'^2 - \omega^2 + i\eta}\, d\omega' \qquad (S8b)$$

where Ω is the volume of the primitive cell, q the Bloch wave vector of the incident wave, c and v the conduction and valence states, $\boldsymbol{k}$ the Bloch wave vector used to expand the Kohn-Sham solutions, and $w_{\boldsymbol{k}}$ the k-point weights. The Dirac delta function ensures energy conservation. Equation S8b is the Kramers-Kronig dispersion relation.

We aligned the band edges of CBTO and Bi_2WO_6 by referencing their respective VBM and CBM Kohn-Sham eigenvalues to the average of their oxygen 1s core states. Results suggest that CBTO Cu 3d – O 2p hybridized states will dominate the VBM at the interface (Figure S2). This is likely due to the higher energies of Cu 3d electrons with respect to Bi 6s – O 2p hybridized orbitals at the top of the valence bands.

Supporting Experimental and Theoretical Results

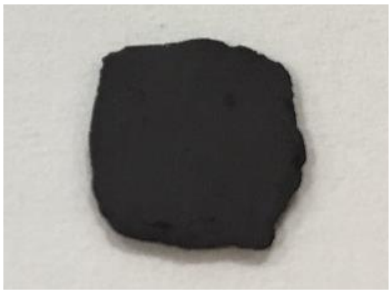

Figure S1. Optical image of pellet formed by starting with powders that had been annealed 4 times in Cu rich atmosphere, pressing these into a Cu box, and annealing again in a tube furnace at 600 °C for 9 hours with 500 sccm flow rate of argon to obtain a dense sintered pellet.

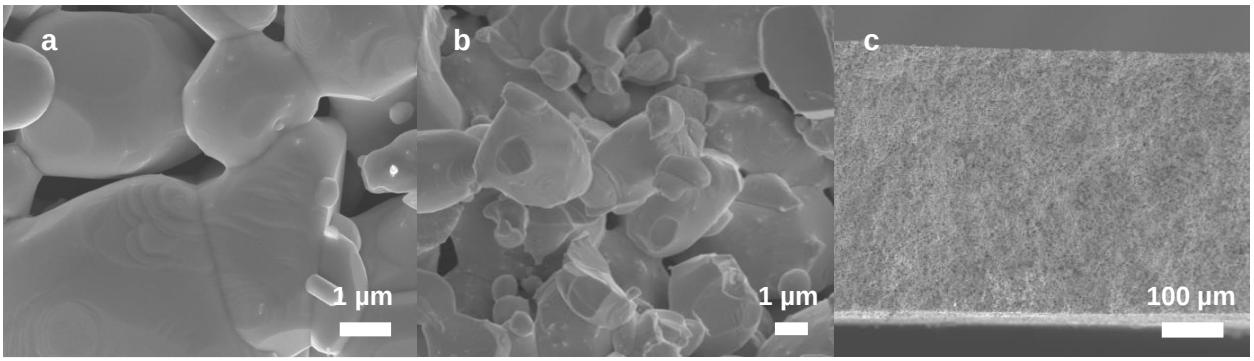

Figure S2. Scanning electron microscopy (SEM) of the pellet from Figure S1 - top (a and b) and cross-section (c) images.

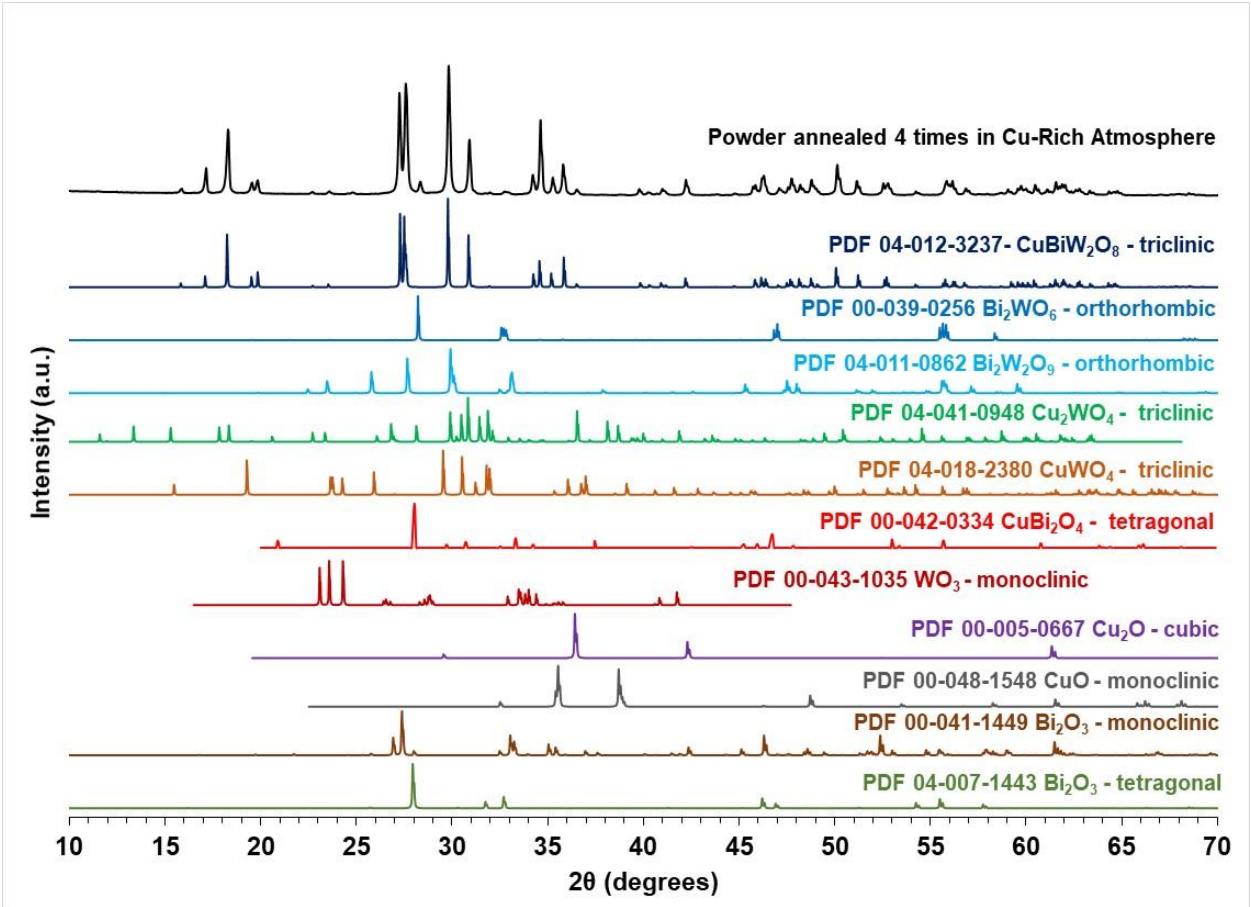

Figure S3. Measured XRD pattern of the powders annealed 4 times in Cu rich atmosphere, and powder diffraction file (PDF) standard patterns of all the phases considered in the XRD analysis ($CuBiW_2O_8$ - triclinic, Bi_2WO_6 - orthorhombic, $Bi_2W_2O_9$ – orthorhombic, Cu_2WO_4 – triclinic, $CuWO_4$ - triclinic, $CuBi_2O_4$ - tetragonal, WO_3 - monoclinic, Cu_2O - cubic, CuO - monoclinic, Bi_2O_3 - monoclinic, and Bi_2O_3 - tetragonal).

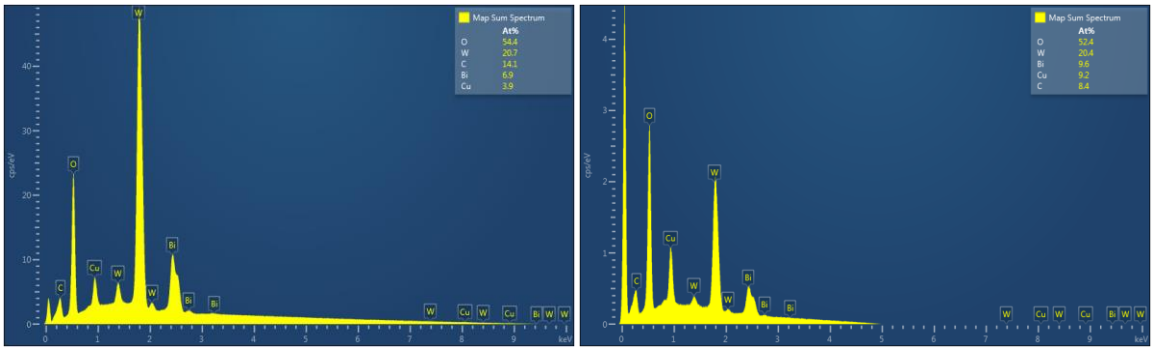

Figure S4. SEM - energy dispersive X-ray spectroscopy (EDS) of powders annealed in Ar without Cu-rich atmosphere (left) and with Cu-rich atmosphere (right).

	Cu	Bi	W	O	C	Total
Stoichiometric $CuBiW_2O_8$	8.3	8.3	16.7	66.7	0.0	100.0
Annealed w/o Cu-rich atm	3.9	6.9	20.7	54.4	14.1	100.0
Annealed w/ Cu-rich atm	9.2	9.6	20.4	52.4	8.4	100.0
Annealed w/o Cu-rich atm excl. C	4.5	8.0	24.1	63.3	0.0	100.0
Annealed w/ Cu-rich atm excl. C	10.0	10.5	22.3	57.2	0.0	100.0

Table S1. EDS comparison of atomic percentage of powders annealed with and without Cu-rich atmosphere.

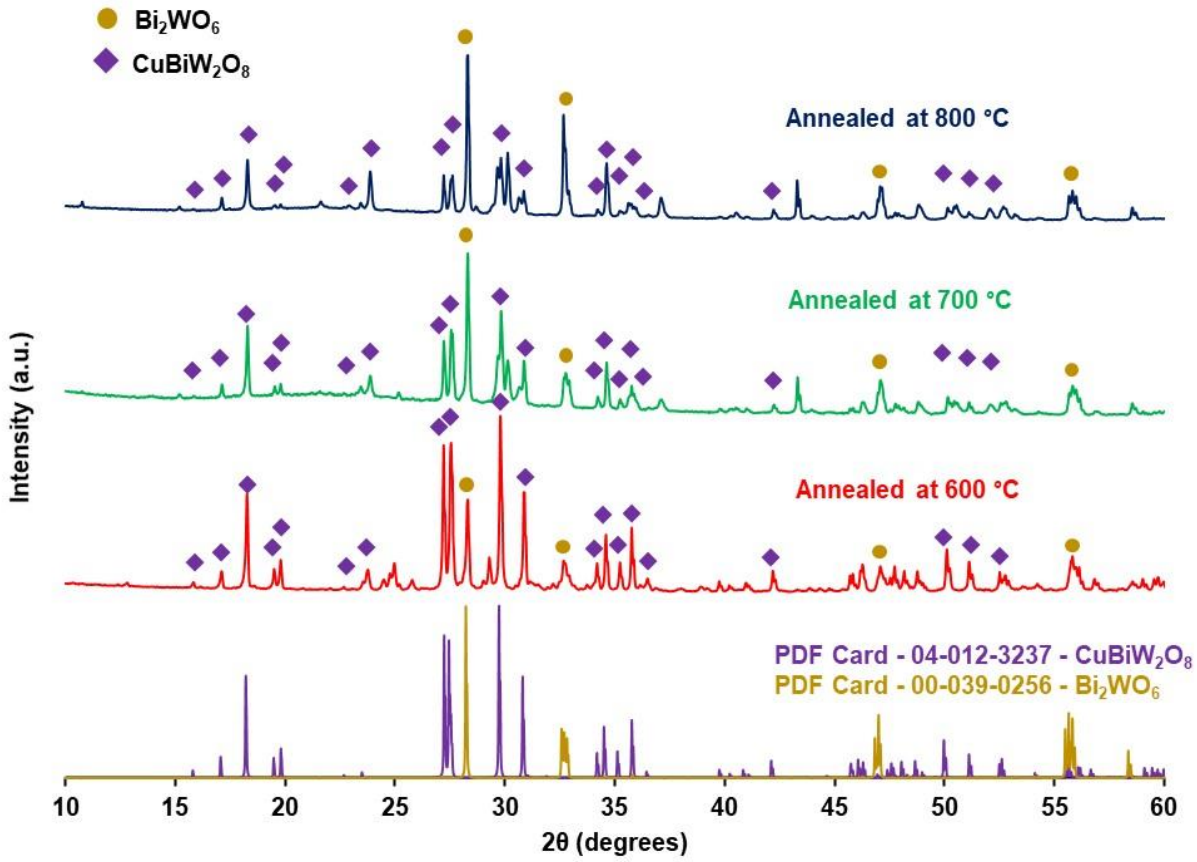

Figure S5. XRD patterns of powders annealed 1 time in Cu-rich atmosphere at temperatures of 600, 700 and 800 °C.

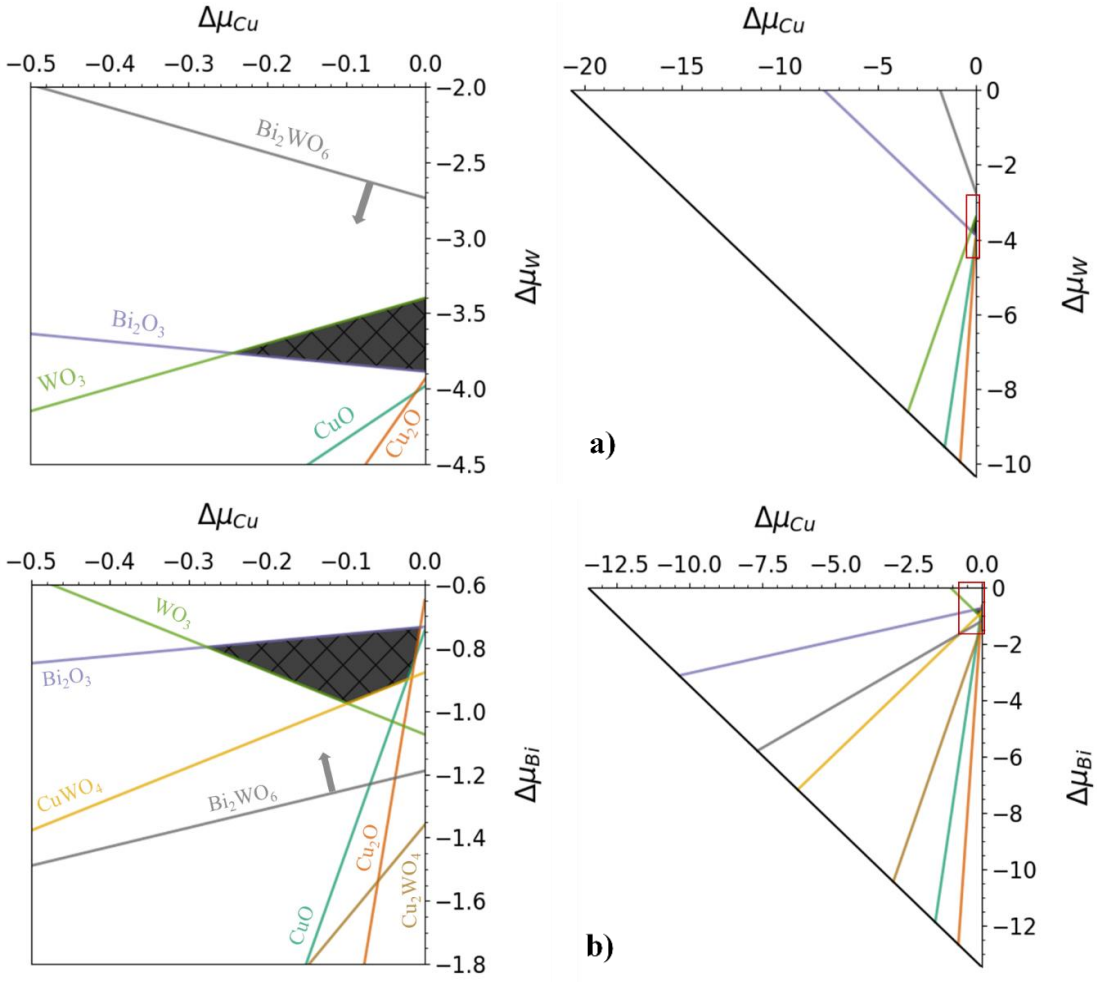

Figure S6. Chemical potential landscape for $CuBiW_2O_8$ (CBTO) as a function of constituent chemical potentials (zoomed at left). Outer bounds represent the entire CBTO thermodynamic stability region. With Bi taken as a free variable (a), $\Delta\mu_{Bi}$ is set to -0.7 eV. For the case of W as the free variable (b), $\Delta\mu_W$ is set to -3.96 eV. The shaded region contains points in which all CBTO fragments are thermodynamically unstable, except for Bi_2WO_6, which is thermodynamically stable in the direction indicated by the arrow (zoomed view). All Cu-containing compounds are calculated using DFT+U with U_{eff} = 6 eV on Cu 3d bands.

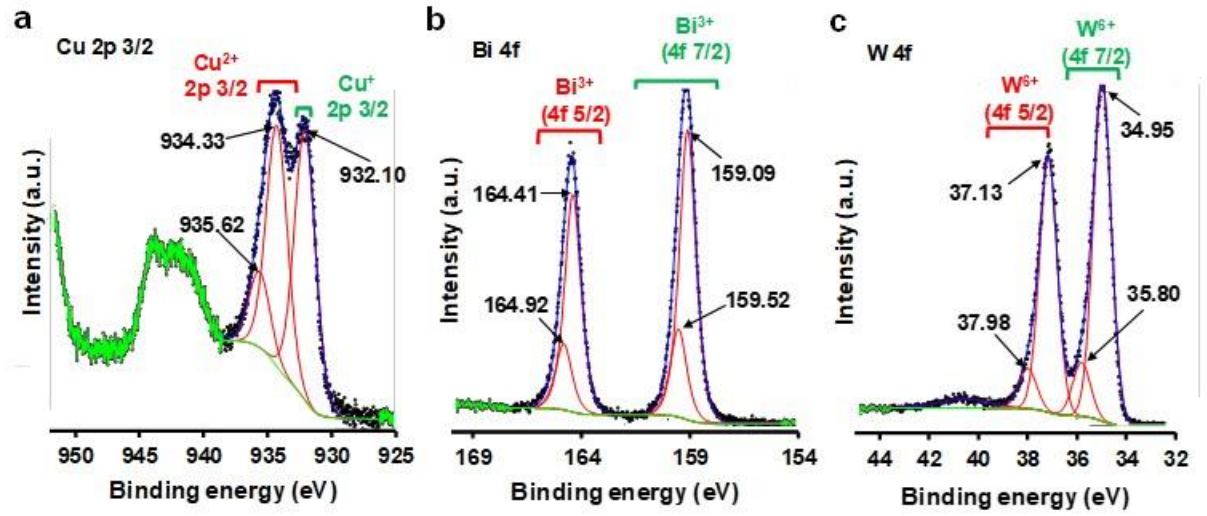

Figure S7. X-ray photoelectron spectra of pellet formed by annealing powders 4 times in Cu-rich conditions, followed by pressing and once again annealing in Cu-rich condition. a) Cu 2p XP spectra, b) Bi 4f XP spectra, c) W 4f XP spectra. Red traces correspond the fitted peaks for Cu 2p, Bi 4f and W 4f regions.

Figure S7a reports the XP spectrum of the Cu 2p region, for which prior studies ascribed peaks in the range of 932.7 - 935.7 eV to the Cu 2p 3/2 features from Cu^{2+} ions in Cu-oxide compounds and 931.6 - 932.8 eV to the corresponding features from Cu^{1+} ions in Cu-oxide compounds.[19-22] We ascribe the fitted peaks at 935.62 eV and 934.33 to Cu^{2+}. In addition, the presence of a strong shake-up peak at 940 – 945 eV is also a clear indication of the presence of Cu^{2+}.[23] The Cu^{2+} signal may come from impurities such as CuO or some other Cu^{2+}-oxide. We ascribe the peak at 932.10 eV to Cu^{1+}, which may come from CBTO or some other Cu^{1+} oxide. For the Bi 4f region in Figure S7b, peaks in the 157.8 - 161.5 eV and peaks in the 163.1 - 166.0 eV range were ascribed to Bi^{3+} 4f 7/2 and 5/2 features, respectively, from Bi-oxide compounds in prior studies.[24, 25] We ascribe fitted peaks at 164.92 eV, 164.41 eV, 159.52 eV and 159.09 eV to Bi^{3+} features, with the two sets of Bi^{3+} peaks likely generated by CBTO and Bi_2WO_6. For the W 4f region in Figure S7c, prior studies ascribed peaks in the 34.5 - 36.6 eV and 37.1 - 39.6 eV range to W^{6+} 4f 7/2 and 5/2 features, respectively, in W-oxide compounds.[26-29] We ascribe the fitted peaks at 37.98 eV, 37.10 eV, 35.80 eV and 34.95 eV to W^{6+} features, with the two sets of peaks likely coming from CBTO and Bi_2WO_6.

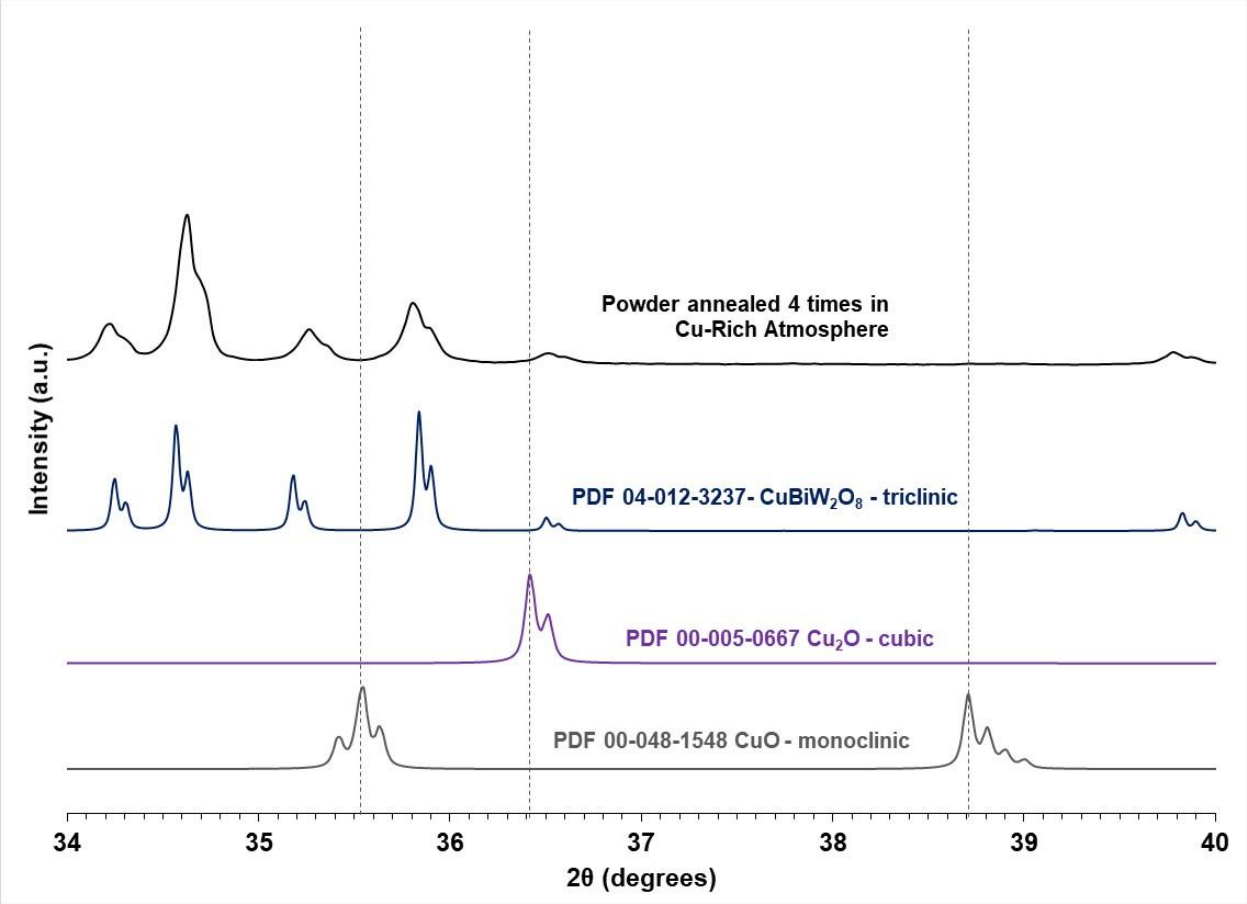

Figure S8. XRD pattern of the 4-times Cu-rich annealed powders expanded in the range of angles in which CuO and Cu_2O have major peaks.

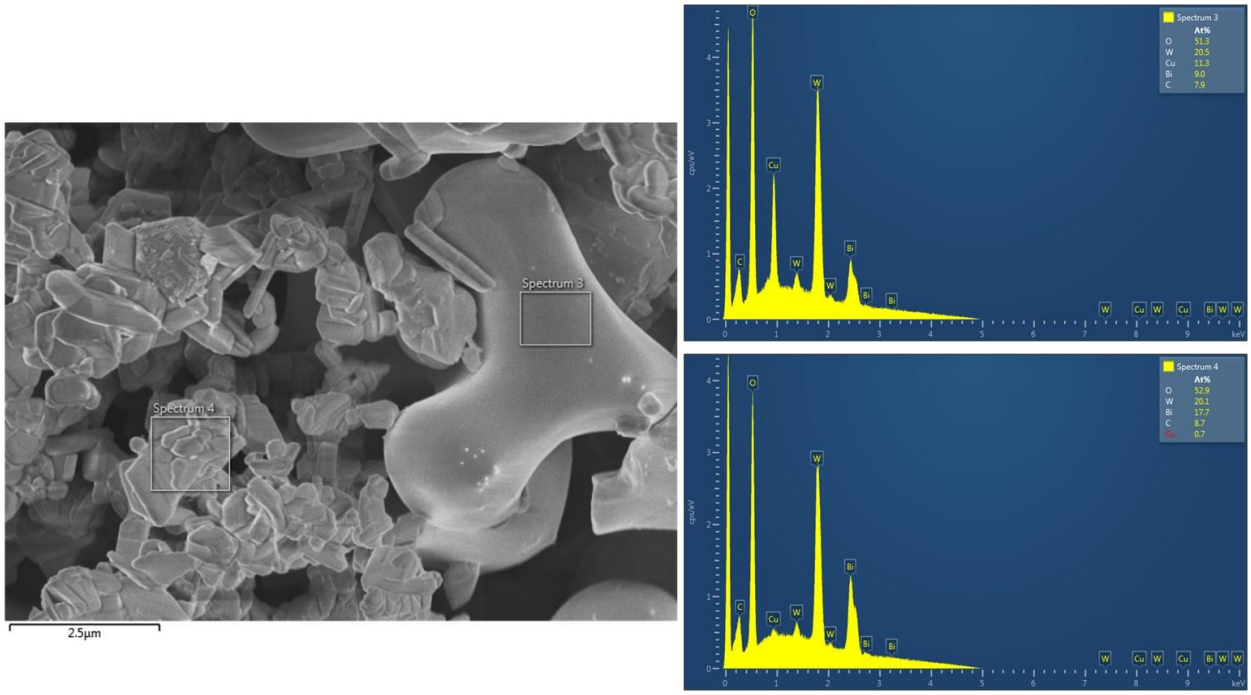

Figure S9. EDS of rounded particles (spectrum at top right) and plate-like particles (spectrum at bottom right) in powders annealed 1 time in Cu-rich atmosphere.

	Cu	Bi	W	O	C	Total
Stoichiometric $CuBiW_2O_8$	8.3	8.3	16.7	66.7	0.0	100.0
Bi_2WO_6	0.0	22.2	11.1	66.7	0.0	100.0
$Bi_2W_2O_9$	0.0	15.4	15.4	69.2	0.0	100.0
Rounded particles	11.3	9.0	20.5	51.3	7.9	100.0
Plate-like particles	0.7	17.7	20.1	52.9	8.7	100.1
Rounded particles excl. C	12.3	9.8	22.3	55.7	0.0	100.0
Plate-like particles excl. C	0.8	19.4	22.0	57.9	0.0	100.1

Table S2. EDS comparison of atomic percentage of rounded and plate-like particles in powders annealed 1 time in Cu-rich atmosphere.

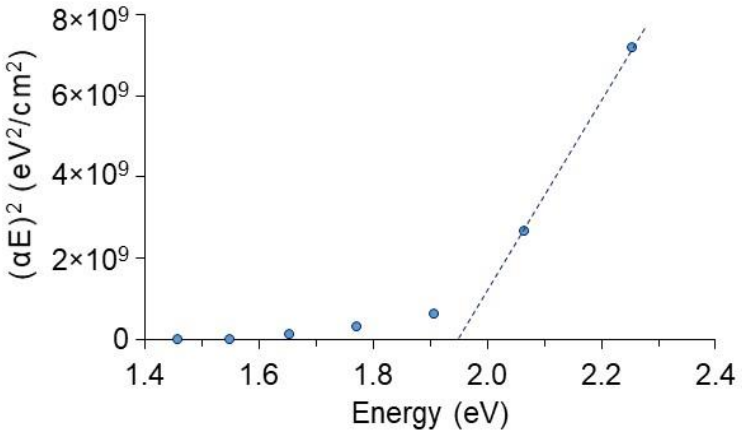

Figure S10. Tauc plot of $(\alpha E)^{1/r}$ vs. E, where E is the photon energy and exponent r = 0.5, calculated from the wavelength-dependent optical absorption of the powders annealed 4 times in Cu-rich atmosphere, dispersed in a solvent, and drop-casted onto quartz substrates.

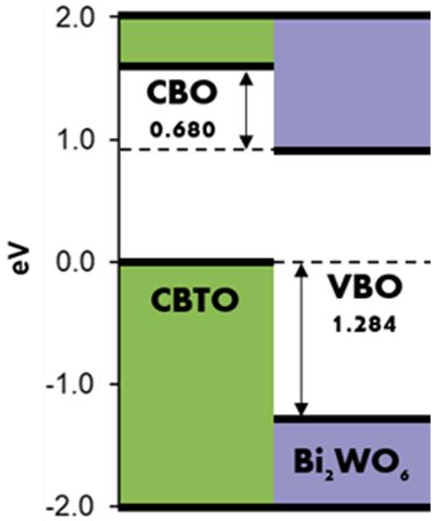

Figure S11. DFT calculated valence and conduction band edges of CBTO and Bi_2WO_6 aligned with respect to the average of the oxygen 1s core states. Oxygen 1s states for each compound were averaged over all O-sites. CBTO (Bi_2WO_6) band edges were shifted up (down) due to the difference between the average 1s state and their respective 1s states. CBTO valence band edge is set at 0 eV. Valence/conduction band offsets (VBO/CBO) are shown.

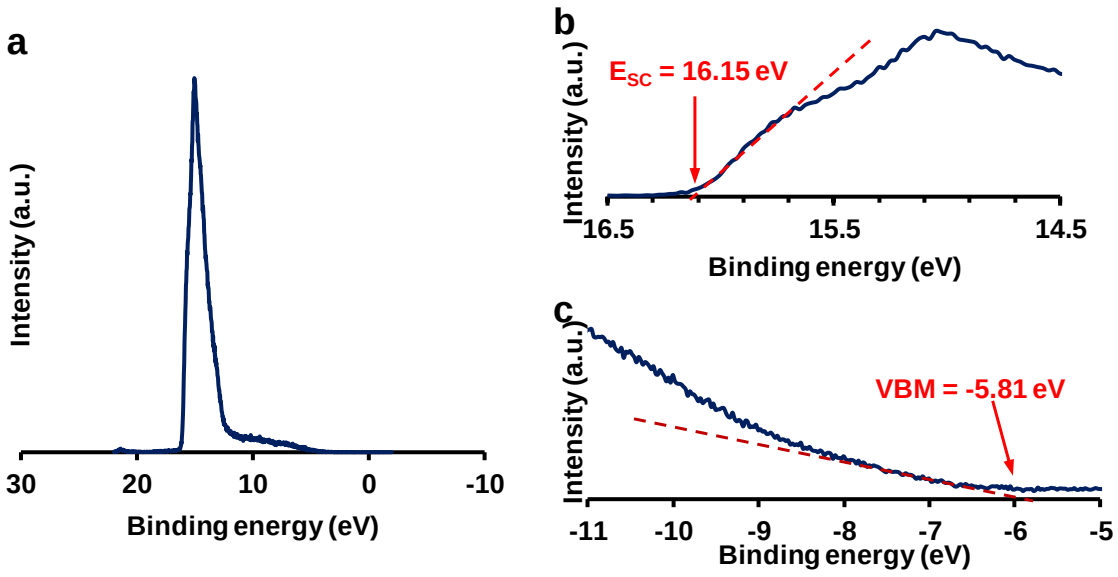

Figure S12. a) ultraviolet photoelectron spectroscopy (UPS) spectrum of sintered powder pellet (annealed 4 times in Cu-rich atmosphere and then pelletized), b) close-up of secondary electron cut off region, and c) close-up of valence band region.

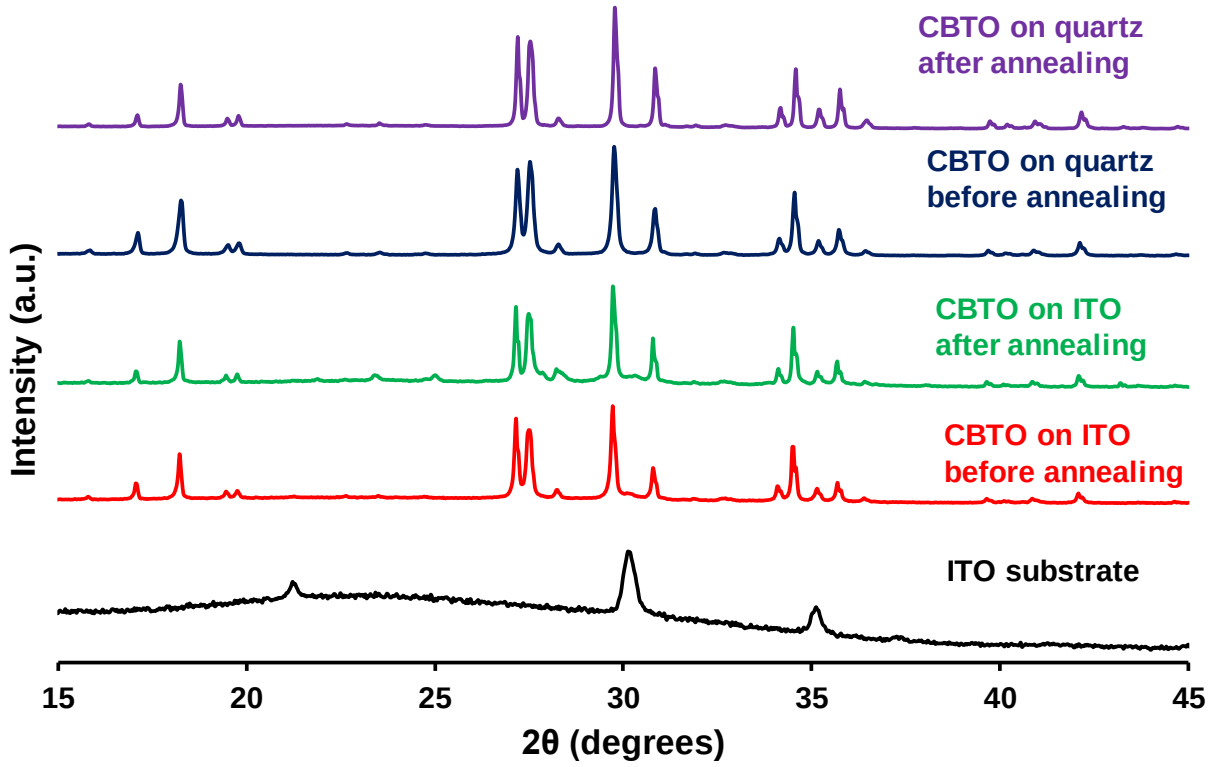

Figure S13. X-ray diffraction of ITO substrate (black), CBTO powders on quartz before (red) and after (green) annealing, CBTO powders on ITO before (blue) and after (purple) annealing.

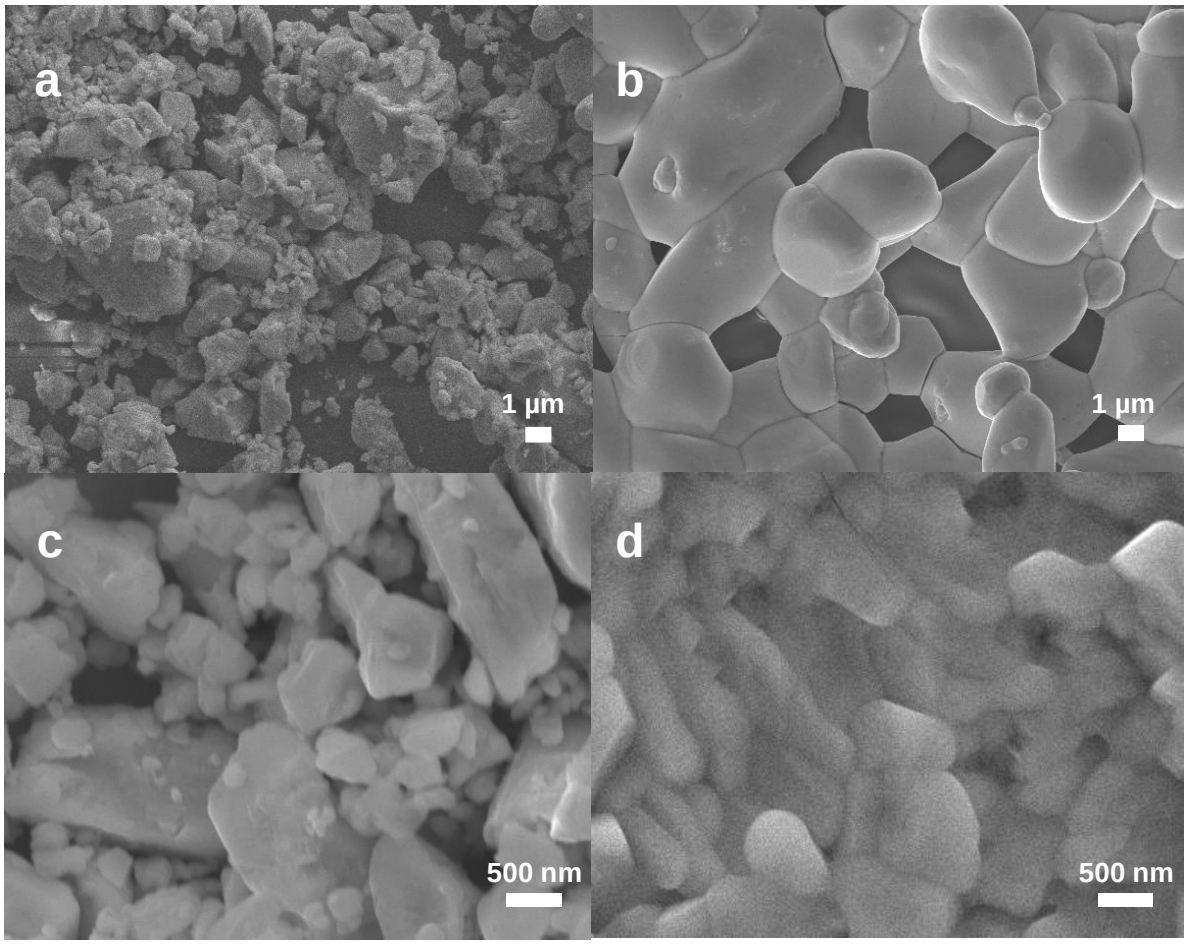

Figure S14. Scanning electron microscopy (SEM) top images of CBTO powders on quartz a) before and b) after annealing, and CBTO powders on ITO c) before and d) after annealing.

References

1. Kresse, G.; Furthmüller, J., Efficient iterative schemes for ab initio total-energy calculations using a plane-wave basis set. *Physical Review B* **1996,** *54* (16), 11169-11186.

2. Kresse, G.; Furthmüller, J., Efficiency of ab-initio total energy calculations for metals and semiconductors using a plane-wave basis set. *Computational Materials Science* **1996,** *6* (1), 15-50.

3. Perdew, J. P.; Chevary, J. A.; Vosko, S. H.; Jackson, K. A.; Pederson, M. R.; Singh, D. J.; Fiolhais, C., Atoms, molecules, solids, and surfaces: Applications of the generalized gradient approximation for exchange and correlation. *Physical Review B* **1992,** *46* (11), 6671-6687.

4. Perdew, J. P.; Burke, K.; Ernzerhof, M., Generalized Gradient Approximation Made Simple. *Physical Review Letters* **1996,** *77* (18), 3865-3868.

5. Kohn, W.; Sham, L. J., Self-Consistent Equations Including Exchange and Correlation Effects. *Physical Review* **1965,** *140* (4A), A1133-A1138.

6. Kresse, G.; Joubert, D., From ultrasoft pseudopotentials to the projector augmented-wave method. *Physical Review B* **1999,** *59* (3), 1758-1775.

7. Blöchl, P. E., Projector augmented-wave method. *Physical Review B* **1994,** *50* (24), 17953-17979.

8. Methfessel, M.; Paxton, A. T., High-precision sampling for Brillouin-zone integration in metals. *Physical Review B* **1989,** *40* (6), 3616-3621.

9. Monkhorst, H. J.; Pack, J. D., Special points for Brillouin-zone integrations. *Physical Review B* **1976,** *13* (12), 5188-5192.

10. Sarker, P.; Prasher, D.; Gaillard, N.; Huda, M. N., Predicting a new photocatalyst and its electronic properties by density functional theory. *Journal of Applied Physics* **2013,** *114* (13), 133508.

11. Anisimov, V. I.; Zaanen, J.; Andersen, O. K., Band theory and Mott insulators: Hubbard U instead of Stoner I. *Physical Review B* **1991,** *44* (3), 943-954.

12. Anisimov, V. I.; Solovyev, I. V.; Korotin, M. A.; Czyżyk, M. T.; Sawatzky, G. A., Density-functional theory and NiO photoemission spectra. *Physical Review B* **1993,** *48* (23), 16929-16934.

13. Solovyev, I. V.; Dederichs, P. H.; Anisimov, V. I., Corrected atomic limit in the local-density approximation and the electronic structure of d impurities in Rb. *Physical Review B* **1994,** *50* (23), 16861-16871.

14. Zhou, F.; Marianetti, C. A.; Cococcioni, M.; Morgan, D.; Ceder, G., Phase separation in Li_xFePO_4 induced by correlation effects. *Physical Review B* **2004,** *69* (20), 201101.

15. Ganduglia-Pirovano, M. V.; Hofmann, A.; Sauer, J., Oxygen vacancies in transition metal and rare earth oxides: Current state of understanding and remaining challenges. *Surface Science Reports* **2007,** *62* (6), 219-270.

16. Sarker, P.; Al-Jassim, M. M.; Huda, M. N., Theoretical limits on the stability of single-phase kesterite-Cu_2ZnSnS_4. *Journal of Applied Physics* **2015,** *117* (3), 035702.

17. Akkus, H.; Mamedov, A. M., Ab initio calculations of the electronic structure and linear optical properties, including self-energy effects, for paraelectric SbSI. *Journal of Physics: Condensed Matter* **2007,** *19* (11), 116207.

18. Gajdoš, M.; Hummer, K.; Kresse, G.; Furthmüller, J.; Bechstedt, F., Linear optical properties in the projector-augmented wave methodology. *Physical Review B* **2006,** *73* (4), 045112.

19. Haber, J.; Machej, T.; Ungier, L.; Ziółkowski, J., ESCA studies of copper oxides and copper molybdates. *Journal of Solid State Chemistry* **1978,** *25* (3), 207-218.

20. Ghijsen, J.; Tjeng, L. H.; van Elp, J.; Eskes, H.; Westerink, J.; Sawatzky, G. A.; Czyzyk, M. T., Electronic structure of Cu_2O and CuO. *Physical Review B* **1988,** *38* (16), 11322-11330.

21. Moretti, G.; Fierro, G.; Lo Jacono, M.; Porta, P., Characterization of CuO–ZnO catalysts by X-ray photoelectron spectroscopy: Precursors, calcined and reduced samples. *Surface and Interface Analysis* **1989,** *14* (6-7), 325-336.

22. Sacher, E.; Klemberg-Sapieha, J. E.; Cambron, A.; Okoniewski, A.; Yelon, A., X-ray photoelectron spectroscopic evidence for CuIII in superconducting $YBa_2Cu_3O_7$ ceramic. *Journal of Electron Spectroscopy and Related Phenomena* **1989,** *48* (2), C7-C12.

23. Poulston, S.; Parlett, P. M.; Stone, P.; Bowker, M., Surface Oxidation and Reduction of CuO and Cu_2O Studied Using XPS and XAES. *Surface and Interface Analysis* **1996,** *24* (12), 811-820.

24. Kazushige, O.; Kenji, Y.; Masatoshi, A.; Yoshiaki, T.; Hisao, H., Bismuth Valence Studies of As-Grown Superconducting Bi-Sr-Ca-Cu-O Thin Films with T c(zero) from 98 K to 66 K. *Japanese Journal of Applied Physics* **1992,** *31* (7B), L953.

25. Ismail, F. M.; Hanafi Z, M., Some Physico-Chemical Properties of Bismuth Chalcogenides x-Ray Photoelectron and Diffuse Reflectance Spectra. In *Zeitschrift für Physikalische Chemie*, 1986; Vol. 267O, p 667.

26. Shi, J.; Allara, D. L., Characterization of High-Temperature Reactions at the BaO/W Interface. *Langmuir* **1996,** *12* (21), 5099-5108.

27. McGuire, G. E.; Schweitzer, G. K.; Carlson, T. A., Core electron binding energies in some Group IIIA, VB, and VIB compounds. *Inorganic Chemistry* **1973,** *12* (10), 2450-2453.

28. Chowdari, B. V. R.; Tan, K. L.; Chia, W. T., Raman and X-ray photoelectron spectroscopic studies of lithium phosphotungstate glasses. *Solid State Ionics* **1992,** *53-56*, 1172-1178.

29. Halada, G. P.; Clayton, C. R., Comparison of Mo–N and W–N synergism during passivation of stainless steel through x-ray photoelectron spectroscopy and electrochemical analysis. *Journal of Vacuum Science & Technology A* **1993,** *11* (4), 2342-2347.